Journal of Dynamic Systems, Measurement and Control. Received September 25, 2015;
Accepted manuscript posted May 29, 2018. doi:10.1115/1.4040440

Hybrid Analog/Digital Control of Bilateral Teleoperation Systems

Ting Yang [1, 2, 3], Junfeng Hu [1], Wei Geng [1], Dan Wang [1], Yili Fu [* 2], Mahdi Tavakoli [* 3]

1 School of Medicine information, Xuzhou Medical University, Xuzhou, Jiangsu, 221004, China yixinyt@xzhmu.edu.cn,

2 State Key Laboratory of Robotics and Systems, Harbin Institute of Technology, Harbin, Heilongjiang, 150080, China ylfms@hit.edu.cn,

3 Department of Electrical and Computer Engineering, University of Alberta, T6G 2V4, Edmonton, Alberta, Canada mahdi.tavakoli@ualberta.ca

* is corresponding author

Hybrid Analog/Digital Control of Bilateral Teleoperation Systems

Abstract: Hybrid analog/digital control of bilateral teleoperation systems can lead to superior performance (transparency) while maintaining stability compared to pure analog or digital control methods. Such hybrid control is preferable over pure analog control, which is inflexible and not ideal for realizing complex teleoperation control algorithms, and pure digital control, which restricts teleoperation performance due to a well-known stability-imposed upper bound on the product of the digital controller's proportional gain and the sampling period. In this paper, a hybrid controller combining a Field Programmable Analog Array (FPAA) based analog controller and a personal computer based digital controller is compared in terms of performance and stability to its analog and digital counterparts. A stability analysis indicates that the addition of analog derivative term widens the range of teleoperation controls gains that satisfy the stability conditions, paving the way for improving the teleoperation performance. We also show how the hybrid controller leads to better teleoperation performance. To this end, we study the human's performance of a switch flipping task and a stiffness discrimination task in the teleoperation mode. In both tasks, the hybrid analog/digital controller allows the human operators to achieve the highest task success rates.

Keywords: Bilateral teleoperation; analog control; digital control; stability; transparency; task performance

1: Introduction

In a bilateral teleoperation system, a human operator interacts with a user interface ("master"), which transfers the operator's action to a robot ("slave"). Once the slave makes contact with an environment to accomplish a required task, the environment's reaction is displayed in the form of forces to the human operator's hand via the master. A bilateral teleoperation system minus the human operator and the environment is called a bilateral teleoperator, and consists of the master, the slave, the controller, and the communication channel between the master and the slave.

In a bilateral teleoperation system, the controller should not only make the system stable but it should also ensure the system has high performance (transparency). Transparency measures the extent to which a human operator performing a task via a teleoperation system feels as if he/she is performing the

same task in a direct-touch mode. As discussed below, both the stability and the transparency of a bilateral teleoperation system can be jeopardized by discretization of the controller [1].

Digital control design techniques have liberated control designers from time-consuming analog control design. However, this has come at the cost of losing the advantages of analog control and potential stability consequences [2-7]. When an analog controller is discretized, its states are not updated during the hold periods, regardless of the changes in the states of the original analog controller. Considering the most widely used hold function, namely the Zero-Order-Hold (ZOH), the states stay at their latest values, which means the control actions keep constant for the entire sampling period. This introduces a difference between the energy generated by a digital controller and the one generated by the original analog controller, and can lead to severe stability problems and passivity violations. Such energy difference is often referred to as energy leak in bilateral teleoperation systems [8].

In order to account for the adverse influence of such energy leaks caused by discretization and ensure the stability of bilateral teleoperation systems, different approaches can be taken. Papers have either modified the teleoperation controllers to ensure the digitally controlled system's stability [9], or have analyzed the stability of the sampled-data system with discretized controllers [10]. Leung and Francis' research [9] shows there exists an upper bound on the sampling period to keep the system stable in the step-invariant discretization of the digital controller. As for stability analysis of the sampled-data teleoperation system, research has considered the passivity of the teleoperator [11, 12] or the less-conservative absolute stability of the teleoperator [10]. Other approaches consider the absolute stability of the digital communication channel [13] or the stability of the overall teleoperation system for known models of the slave robot's environment [14].

Besides teleoperation stability, teleoperation transparency is also undermined by controller discretization. As shown in [10], in a digitally controlled position-error-based teleoperation system, the teleoperator's absolute stability condition imposes a trade-off between the sampling period and the

proportional gain of the PD teleoperation controller. On the other hand, high teleoperation transparency generally requires using high gains in the PD controller. The above means a trade-off between stability and transparency of a teleoperation system: A larger control gain leads to higher transparency but may jeopardize the stability of the sampled-data teleoperation system. One way of solving this problem is to use fast-sampling processors [15-18], but this option is generally more expensive than ubiquitous personal computers.

To contrast the aforementioned stability/transparency trade-off with that in the case of analog control, the same position-error-based teleoperation system's theoretical absolute stability conditions do not constrain the analog controller gains by any upper bound [10], and therefore do not constrain the transparency. In practice, however, the analog controller is limited by saturations and nonlinearities in the circuits involving operational amplifiers, which lead to upper bounds on the controller gains in a different way. In addition, in some situations such as haptics-based surgical simulation, complex models capturing force/deformation characteristics of soft tissue need to be realized (the virtual environment models in the haptic interaction context play the role of controllers in the haptic teleoperation context). Implementing the algorithms to model complex environments is much easier to with a digital signal processor than with analog hardware.

While the advantages of combined analog/digital control have been investigated for haptic interaction [19], it has not been studied in the context of bilateral teleoperation systems. Limitations imposed by analog control alone or digital control alone and the benefits provided by each one motivates us to consider hybrid analog/digital control of bilateral teleoperation systems in this paper. Despite the huge body of literature in the field of bilateral teleoperation stability analysis, there are few papers that directly tackle the fundamental source of energy leaks, which is the controller discretization. We do so by involving an analog controller and overcome the limitations of that by supplementing the control loop with a digital controller. FPAA is a new type of reconfigurable analog circuits. Among many commercially

available devices [20, 21], the programmable analog arrays from the Anadigm Company are the most popular circuits [21]. In our work, a dpASP device (second-generation of FPAA) AN231E04 from Anadigm is used to implement any analog control. The AnadigmDesigner2 software provides a simple design template for PID control [20].

The proposed hybrid FPAA/digital controller widens the range of control gain under stable conditions. In experiments, the performance of the proposed system shows its superiority by allowing a human operator to perform tasks that are not easily doable with pure analog or digital control.

The control goal in our paper is to stably achieve large enough control gains so that human tasks requiring high transparency can be done successfully. Tasks requiring very high transparency (very large control gains) prohibit the use of digital controlled teleoperation system due to system stability issues. The proposed control architecture can attain the task-required high system transparencies under stable conditions while maintaining the advantages of digital control.

The paper is organized as follows. A typical bilateral teleoperation system is modeled in Section 2. A detailed analysis of stability conditions for hybrid analog/digital control is presented in Section 3. In Section 4, the experimental teleoperation system setup is presented first, the stability range of the teleoperation system with hybrid bilateral controller is shown next, and then two case studies are presented in which the human task performance is compared between the proposed hybrid analog/digital controller, the analog controller, and the digital controller. Lastly, concluding remarks are given in Section 5. Section 6 is our acknowledgement.

2: Modelling of a bilateral teleoperation system with hybrid controllers

In this section, a bilateral typical teleoperation system is modeled and then configured with a hybrid analog/digital controller; see Fig. 1 for the closed-loop position error based (PEB) controlled teleoperation system. In this paper, the PEB teleoperation control method is chosen because, for direct force reflection

(DFR) control, even an analog controlled teleoperation system will not be absolutely stable [10]. Since the study of the stability-transparency tradeoffs caused by sampling and how they limit task performance is of interest, it is appropriate to start with a known-stable continuous-time teleoperation control architecture, namely the PEB control method.

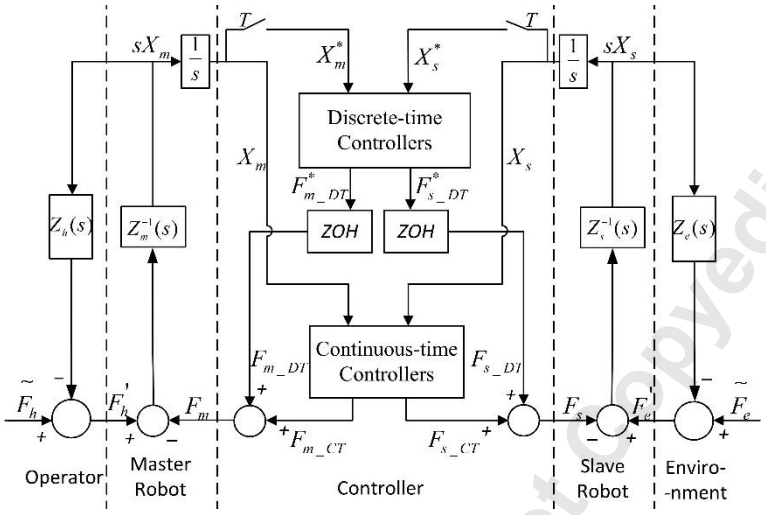

Fig. 1: A PEB bilateral teleoperation system with a hybrid continuous-time (analog) and discrete-time (digital) controller.

Here, $F_h^{'}$ is the interaction force between the master robot and the human operator, and $F_e^{'}$ is the interaction force between the slave robot and the environment. Also, $\tilde{F}_h$ and $\tilde{F}_e$ represent the exogenous human operator and environment forces, respectively. $F^*_{m\_DT}$ and $F^*_{s\_DT}$ are the digital controllers outputs, which are converted to analog (F_{m_DT} and F_{s_DT}) through Zero-Order-Hold (ZOH), while F_{m_CT} and F_{s_CT} are outputs of the analog controllers. X_m and X_s denote the position of the master and slave robots, which are converted to digital (X_m^* and X_s^*) using sampler blocks. Z_h and Z_e are the operator and environment impedances, respectively. Z_m, Z_s represent the impedances of the master and slave robots.

The dynamic models of the human operator and the environment are:

$$\begin{aligned} \tilde{F}_h - F_h^{'} &= Z_h(\mathrm{s}) \cdot sX_m \,, \\ \tilde{F}_e - F_e^{'} &= Z_e(\mathrm{s}) \cdot sX_s \,, \end{aligned} \tag{1}$$

where s is the Laplace operator. The dynamics of the master and slave robots in the s-domain are:

$$\begin{aligned} sX_m &= Z_m(-F_m + F_h^{'}) \,, \\ sX_s &= Z_s(-F_s + F_e^{'}) \,, \end{aligned} \tag{2}$$

where $F_m = F_{m\_DT} + F_{m\_CT}$ and $F_s = F_{s\_DT} + F_{s\_CT}$ are the control signals for the master and the slave robots, respectively. The master and slave impedances are considered to be

$$\begin{aligned} Z_m^{-1} &= \frac{1}{m_m s + b_m} \,, \\ Z_s^{-1} &= \frac{1}{m_s s + b_s} \,, \end{aligned} \tag{3}$$

where m_m and m_s denote the masses of the master and slave robots, respectively, and b_m and b_s denote the corresponding damping terms.

For the digital controllers, the analog signals X_m and X_s are sampled at time instants separated by T as [22]

$$X^*(s) = \sum_{k=0}^{\infty} x(kT) e^{-skT} \,, \tag{4}$$

The z-domain equivalent of (3) is $X(z) = X^*(s)\big|_{s=1/T \ln z}$. The Zero-Order-Hold (ZOH) blocks are used to convert the output of a digital controller to analog with the transfer function

$$G_h(s) = \left(1 - e^{-sT}\right) \Big/ sT \,. \tag{5}$$

Since we are using the PEB teleoperation architecture, the sampled-data outputs of the master and slave controllers are [23]

$$\begin{aligned} F_{m\_DT}^*(s) &= \mathrm{C}_{m\_DT}(z)[X_s^*(s) - X_m^*(s)] \,, \\ F_{s\_DT}^*(s) &= \mathrm{C}_{s\_DT}(z)[X_m^*(s) - X_s^*(s)] \,, \end{aligned} \tag{6}$$

where $*$ shows sampled signals. As far as analog control, the outputs of the master and slave controllers are

$$\begin{aligned} F_{m\_CT}(s) &= \mathrm{C}_{m\_CT}(s)[X_s(s) - X_m(s)], \\ F_{s\_CT}(s) &= \mathrm{C}_{s\_CT}(s)[X_m(s) - X_s(s)], \end{aligned} \tag{7}$$

The proportional-derivative (PD) position controllers $C_{m\_CT} = K_{m\_CT} \cdot s + B_{m\_CT}$ and $C_{s\_CT} = K_{s\_CT} \cdot s + B_{s\_CT}$ for the master and the slave, which will be used in (7), need to be first discretized to get C_{m_DT} and C_{s_DT} in the digital control laws (6). In agreement with [10, 24], to have the z-domain equivalent controllers C_{m_DT} and C_{s_DT}, the backward difference is used to approximate s:

$$\begin{aligned} C_{m\_DT}(z) &= K_{m\_DT} + B_{m\_DT} \cdot \frac{z-1}{Tz}, \\ C_{s\_DT}(z) &= K_{s\_DT} + B_{s\_DT} \cdot \frac{z-1}{Tz}. \end{aligned} \tag{8}$$

3: Stability analysis of hybrid controlled bilateral teleoperation system

3.1: Mathematical Preliminaries

Definition 1. [25] Let A be a Hermitian symmetric matrix. A is positive semi definite (positive definite) if all of its leading principle minors are non-negative (positive).

Definition 2. [25] The memory-less system $y = h(t,u)$ is passive if $u^T y \geq 0$. Otherwise, it is active (non-passive).

Definition 3. [25] An $m \times m$ proper rational transfer function matrix $G(z)$ is positive real if

Poles of all elements of $G(z)$ are inside or on the unit circle.

For all real ω for which $e^{j\omega T}$ is not a pole of any element of $G(z)$, the matrix $G\left(e^{j\omega T}\right) + G^T\left(e^{-j\omega T}\right)$ is positive semidefinite, and

The poles of any element of $G(z)$ on $|z|=1$ are simple and the associated residue matrices of these poles are positive semidefinite.

The transfer function $G(z)$ is strictly positive real if $G(e^{j(\omega-\omega_0)T})$ is positive real for some $\omega_0 > 0$.

Theorem 1. [25] The LTI minimal realization

$$x(i+1) = Ax(i) + Bu(i) \tag{9}$$

$$y(i) = Cx(i) + Du(i) \tag{10}$$

with $G(z) = C(zI - A)^{-1}B + D$ is passive (strictly passive) if $G(z)$ is positive real (strictly positive real).

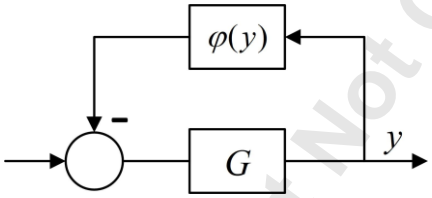

Fig. 2: A sampled-data feedback system with LTI system G in the forward path and nonlinearity $\varphi = \varphi(y)$ in the feedback path.

Theorem 2. [26] Consider a sampled-data multivariable control system that consists of an LTI system in the forward path and the nonlinearity $\varphi = \varphi(y)$ in the feedback path as shown in Fig. 2. Such a system can be represented by

$$x(i+1) = Ax(i) - B\varphi(y) \tag{11}$$

$$y(i) = Cx(i), \quad y \in R^m \tag{12}$$

$$\varphi(y) = [\varphi_1(y_1), \varphi_2(y_2), ..., \varphi_m(y_m)]^T \tag{13}$$

Journal of Dynamic Systems, Measurement and Control. Received September 25, 2015;
Accepted manuscript posted May 29, 2018. doi:10.1115/1.4040440

For any passive $\varphi(y)$, if

$$C(zI-A)^{-1}B \tag{14}$$

is strictly positive real (and, according to Theorem 1, strictly passive), then the system (11)-(13) is stable. This is also referred to as absolute stability of $G(z)$.

3.2: Stability Analysis of a Bilateral Teleoperation System with a Hybrid Controller

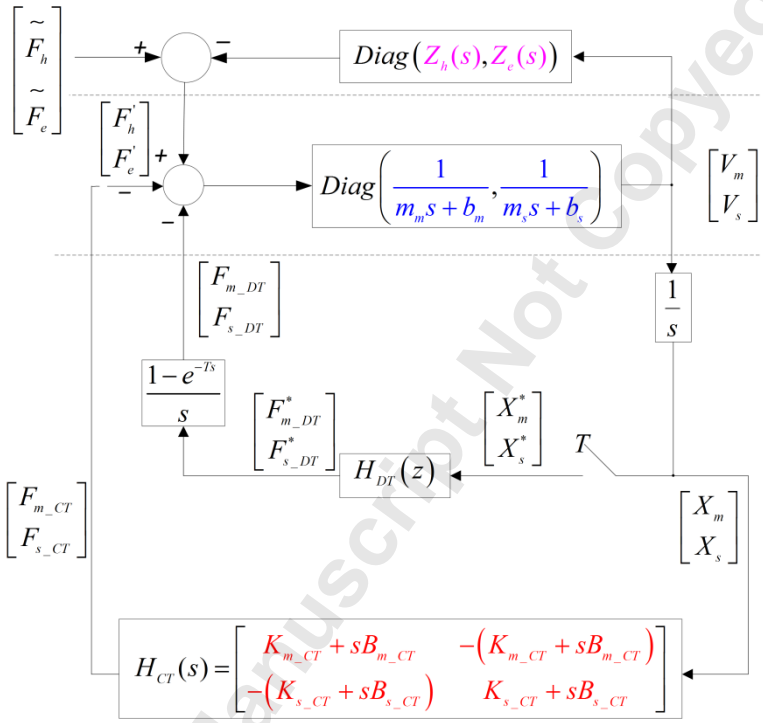

Fig. 3: Block diagram of the hybrid-control PEB bilateral teleoperation system.

Journal of Dynamic Systems, Measurement and Control. Received September 25, 2015;
Accepted manuscript posted May 29, 2018. doi:10.1115/1.4040440

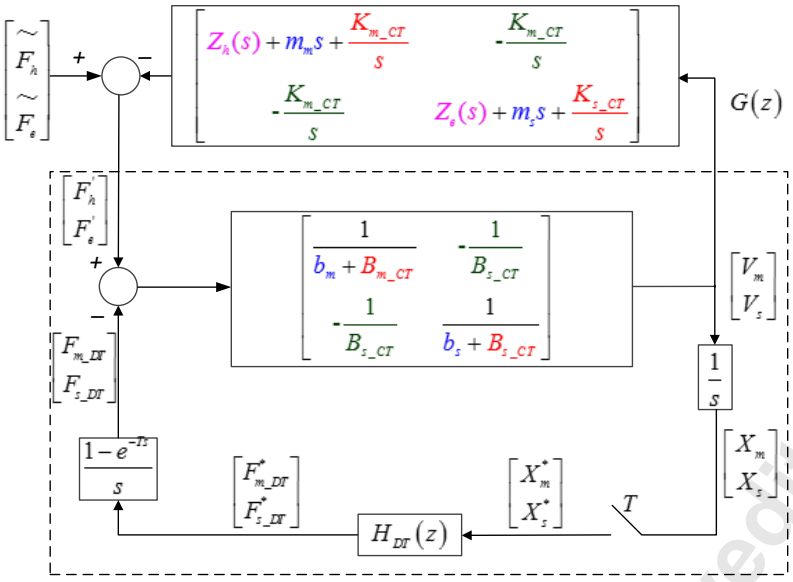

Fig. 4: Modified block diagram of Fig. 3.

Based on (3), (5), (6) and (7), the system in Fig. 1 can be represented as the block diagram in Fig. 3, where

$$H_{CT}(s)=\begin{bmatrix} C_{m\_CT} & -C_{m\_CT} \\ -C_{s\_CT} & C_{s\_CT} \end{bmatrix} = \begin{bmatrix} K_{m\_CT}+sB_{m\_CT} & -\left(K_{m\_CT}+sB_{m\_CT}\right) \\ -\left(K_{s\_CT}+sB_{s\_CT}\right) & K_{s\_CT}+sB_{s\_CT} \end{bmatrix}, \tag{15}$$

$$H_{DT}(z)=\begin{bmatrix} C_{m\_DT} & -C_{m\_DT} \\ -C_{s\_DT} & C_{s\_DT} \end{bmatrix} = \begin{bmatrix} K_{m\_DT}+B_{m\_DT}\cdot\frac{z-1}{Tz} & -\left(K_{m\_DT}+B_{m\_DT}\cdot\frac{z-1}{Tz}\right) \\ -\left(K_{s\_DT}+B_{s\_DT}\cdot\frac{z-1}{Tz}\right) & K_{s\_DT}+B_{s\_DT}\cdot\frac{z-1}{Tz} \end{bmatrix}, \tag{16}$$

In Fig. 3 and Fig. 4, $V_m = sX_m$ and $V_s = sX_s$ denote the velocities of the master and slave robots. Simple but very useful manipulations in Fig. 3can result in the equivalent block diagram in Fig. 4. Note that with the use of velocities instead of positions in (6) and (7), factors of $1/s$ have been introduced in the position controllers. By moving the masses of the master and slave robots (m_m and m_s) and the proportional terms of the master's and slave's analog controllers ($\frac{K_{m\_CT}}{s}$ and $\frac{K_{s\_CT}}{s}$ after factoring in $1/s$) to the operator

and environment impedances, the closed-loop transfer matrix will not change. Similarly, the system is unchanged if the derivative terms of the master's and slave's analog controllers (B_{m_CT} and B_{s_CT}) are moved to the master and slave impedances.

Then, the mapping for the system in Fig. 4 can be written as

$$\begin{bmatrix} F_h^{'}(z) \\ F_e^{'}(z) \end{bmatrix} = \begin{bmatrix} b_m + B_{m\_CT} & -B_{s\_CT} \\ -B_{s\_CT} & b_s + B_{s\_CT} \end{bmatrix} \begin{bmatrix} V_m(z) \\ V_s(z) \end{bmatrix} + H_{DT}(z) \mathrm{Z} \begin{bmatrix} V_m(s)/s \\ V_s(s)/s \end{bmatrix}^{*} \tag{17}$$

It is important to note that $Z\left[\frac{V}{s}\right] \neq Z\left[\frac{1}{s}\right] V(z)$. To be able to derive the transfer function from force to velocity, we need to approximate $Z\left[\frac{V}{s}\right]$. We can do so based on one of the available approximations including forward difference, backward difference and Tustin transformation.

Using the forward difference approximation method, the force to velocity mapping (17) is approximated by

$$\begin{bmatrix} F_h^{'}(z) \\ F_e^{'}(z) \end{bmatrix} = \left(\begin{bmatrix} b_m + B_{m\_CT} & -B_{m\_CT} \\ -B_{s\_CT} & b_s + B_{s\_CT} \end{bmatrix} + H_{DT}(z) \frac{T}{z-1} \right) \begin{bmatrix} V_m(z) \\ V_s(z) \end{bmatrix} = G^{-1}(z) V(z) \tag{18}$$

where

$$G^{-1}(z) = \begin{bmatrix} b_m + B_{m\_CT} + K_{m\_DT} \cdot \frac{T}{z-1} + B_{m\_DT} \cdot \frac{1}{z}, & \\ -K_{m\_DT} \cdot \frac{T}{z-1} - B_{m\_DT} \cdot \frac{1}{z} - B_{m\_CT}; & \\ -K_{s\_DT} \cdot \frac{T}{z-1} - B_{s\_DT} \cdot \frac{1}{z} - B_{s\_CT}, & \\ b_s + B_{s\_CT} + K_{s\_DT} \cdot \frac{T}{z-1} + B_{s\_DT} \cdot \frac{1}{z} & \end{bmatrix} \tag{19}$$

Now, if the operator and the environment impedances in Fig. 3 are passive, so will be the augmented operator and environment blocks in Fig. 4. Thus, based on Theorem 2, the PEB bilateral teleoperation system is stable if $G(z)$ is strictly positive real. As the strict passivity of $G(z)$ is equivalent to the strict passivity of $G^{-1}(z)$, $G^{-1}(z)$ needs to be strictly positive real [27]. Therefore, $G^{-1}(z)$ needs to be checked against Definition 3. According to the first condition in Definition 3, all poles of $G^{-1}(z)$ should be inside or on the unit circle of z, which is satisfied here with one simple pole at the origin and another at $z=1$ in $G^{-1}(z)$ found from (19). For the $z=1$ pole of $G^{-1}(z)$, considering the third condition of Definition 3 for strict positive realness, the residue matrix corresponding to this pole must be positive definite. For (18), the residue matrix is

$$R_0 = \begin{bmatrix} K_{m\_DT}\cdot T & -K_{m\_DT}\cdot T \\ -K_{s\_DT}\cdot T & K_{s\_DT}\cdot T \end{bmatrix} \tag{20}$$

which is clearly positive definite since $K_{m\_DT}, K_{s\_DT}, T>0$ and $\det(R_0)=0$. The last condition needs to be satisfied in Definition 3 is the second condition, which requires $G^{-1}(e^{j(\omega-\omega_0)T})+G^{-T}(e^{-j(\omega-\omega_0)T})$ to be positive definite. Substituting $z=\cos((\omega-\omega_0)T)+j\sin((\omega-\omega_0)T)$, the sum $G^{-1}(e^{j(\omega-\omega_0)T})+G^{-T}(e^{-j(\omega-\omega_0)T})$ needs to be positive definite. Based on Definition 2, we will need

$$D_m > 0 \tag{21}$$

$$\begin{aligned} &D_m\cdot D_s - \left[B_{Ctotal} + B_{Dtotal}\cos\left((\omega-\omega_0)T\right) - \frac{K_{Dtotal}}{2}\cdot T\right]^2 - \\ &\left[\frac{\left(K_{s\_DT}-K_{m\_DT}\right)}{2}T\cot\left(\frac{(\omega-\omega_0)T}{2}\right) + (B_{s\_DT}-B_{m\_DT})\sin((\omega-\omega_0)T)\right]^2 > 0 \end{aligned} \tag{22}$$

where $D_m = 2b_m + 2B_{m\_CT} - K_{m\_DT}T + 2B_{m\_DT}\cos((\omega-\omega_0)T)$, $D_s = 2b_s + 2B_{s\_CT} - K_{s\_DT}T + 2B_{s\_DT}\cos((\omega-\omega_0)T)$, $B_{Dtotal}=B_{s\_DT}+B_{m\_DT}$, $B_{Ctotal}=B_{s\_CT}+B_{m\_CT}$, $K_{Dtotal}=K_{s\_DT}+K_{m\_DT}$.

For $C_{m\_DT}(z)=C_{s\_DT}(z)=K_{DT}+B_{DT}\cdot\frac{z-1}{Tz}$, B_{Dtotal}=$2B_{DT}$ and K_{Dtotal}=$2K_{DT}$, condition (22) is valid if

$$b_m\cdot b_s+(b_m+b_s)B_{Ctotal}-b_{ms}\cdot B_{Ctotal}-\frac{1}{4}{B_{Ctotal}}^2>(b_m+b_s)\cdot\left[\frac{K_{DT}T}{2}-B_{DT}\cos((\omega-\omega_0)T)\right] \quad (23)$$

where B_{Ctotal}=$B_{s\_CT}+B_{m\_CT}$, $b_{ms}\cdot B_{Ctotal}=b_m\cdot B_{s\_CT}+b_s\cdot B_{m\_CT}$.

For $C_{m\_CT}(z)=C_{s\_CT}(z)=K_{CT}+B_{CT}\cdot s$, B_{Ctotal}=$2B_{CT}$. As frequency $\omega-\omega_0$ can take on any value and thus $\cos((\omega-\omega_0)T)\in(-1,1)$, the worst case of (21) and (23) can be obtained when $\cos((\omega-\omega_0)T)=-1$,

$$\frac{D_m}{2}=b_m+B_{CT}-\frac{K_{DT}T}{2}-B_{DT}>0 \quad (24)$$

$$\frac{b_m\cdot b_s}{b_m+b_s}+B_{CT}>\frac{K_{DT}T}{2}+B_{DT} \quad (25)$$

Finally, choosing $b=\min\left\{b_m,\frac{b_m\cdot b_s}{b_m+b_s}\right\}$, a sufficient condition for absolute stability of the hybrid-controlled PEB bilateral teleoperation system will be

$$b+B_{CT}>\frac{K_{DT}T}{2}+B_{DT} \quad (26)$$

With the help of professional designer AnadigmDesigner2 used in this paper, it is easy to realize $K_{m\_CT}=K_{s\_CT}$, and $B_{m\_CT}=B_{s\_CT}$ for our proposed FPAA-based controller [20]. For the other two approximation methods (backward difference and Tustin [28]), stability conditions were obtained in a similar manner. After analysis, the worst-case most-conservative stability conditions happen when using the forward difference approximation method. Thus (26), is the worst-case condition.

3.3: Discussion

Based on the analysis above, we can see that the hybrid analog/digital control method widens the range of admissible control gains (from a stability perspective) by adding an analog derivative term B_{m_CT} / B_{s_CT} in the left-hand side of the formula. This means that, with the help of the analog controller, the digital controller can involve higher control gains without jeopardizing stability compared to a situation where only a digital controller is present.

The proportional gain of the analog controller does not influence the stability condition (26) in any way. This is a welcome result because the analog proportional gain can be used to recreate contact with highly stiff surfaces without undermining the haptic simulation system's stability (in the haptic interaction context) and employ high-gain slave robot control (in the haptic teleoperation context). In the absence of analog proportional control, (26) puts an upper bound on the digital proportional controller K_{DT}, which limits the maximum stiffness of the virtual environment (in the haptic interaction context) and the slave robot control gain (in the haptic teleoperation context). On the other hand, we cannot solely and always rely on using the analog proportional control gain as saturation of the op-amps in the analog controller occurs when the gains are too high. Thus, sometimes we may still need a digital control gain to get the total gain required for performing a particular task. Once we do so, **if** this digital controller's gains violate the stability condition (26), we will simply add enough analog derivative term B_{m_CT} / B_{s_CT} to fulfill (26).

In summary, each of the proportional and derivative gains of both analog and digital controllers are needed and play unique roles in terms of improving teleoperation transparency while preserving system stability. In the next Section, we show the stability and transparency of the proposed hybrid control system in comparison with pure digital and pure analog control.

4: Experimental results

4.1: Experimental setup

Fig. 5 shows an overview of the experimental setup. The setup consists of two identical Servo SRV-02 Quick Connect Modules (Quanser Inc., Markham, ON, Canada) as1-degreee-of-freedom, revolute-joint master and slave robots. Each of the master and slave modules, which is comprised of a DC motor, a gear, and a potentiometer, is preceded by an inner current control loop so that an outer position control loop which can send torque commands to each robot. While the inner current control loop is always implemented by analog components, the outer-loop position controller can be implemented as a combination of a digital controller and an FPAA-based analog controller. The details of the inner current control loop design can be found in [29].

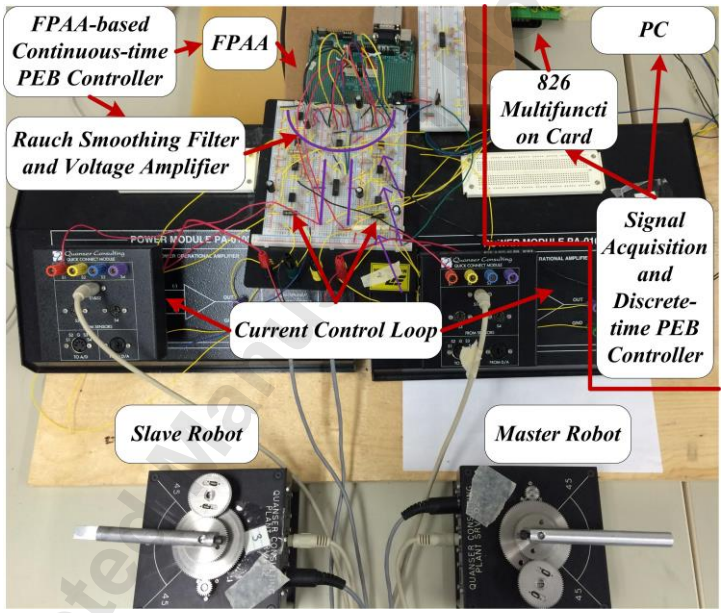

Fig. 5. The experimental bilateral teleoperation system.

Digital signals are processed in a PC with a dual-core Opteron Processor E8400 at 2.99 GHz with a 32-bit Windows 7 operating system. A Model 826 multifunction analog/digital I/O card (Sensoray Co., Tigard, OR, USA) is used for A/D and D/A conversion. First, the master and slave positions are acquired

following A/D conversion of voltages of potentiometers mounted at the robots' joints. Next, the master/slave position error is calculated and fed to the backward-difference digital PD controller in (8) for each of the master and slave robots. Then, following D/A conversion, the final control signals $F_m = F_{m\_DT} + F_{m\_CT}$ and $F_s = F_{s\_DT} + F_{s\_CT}$ are output to the master and slave robots, respectively. The sampling time is 1ms at minimum.

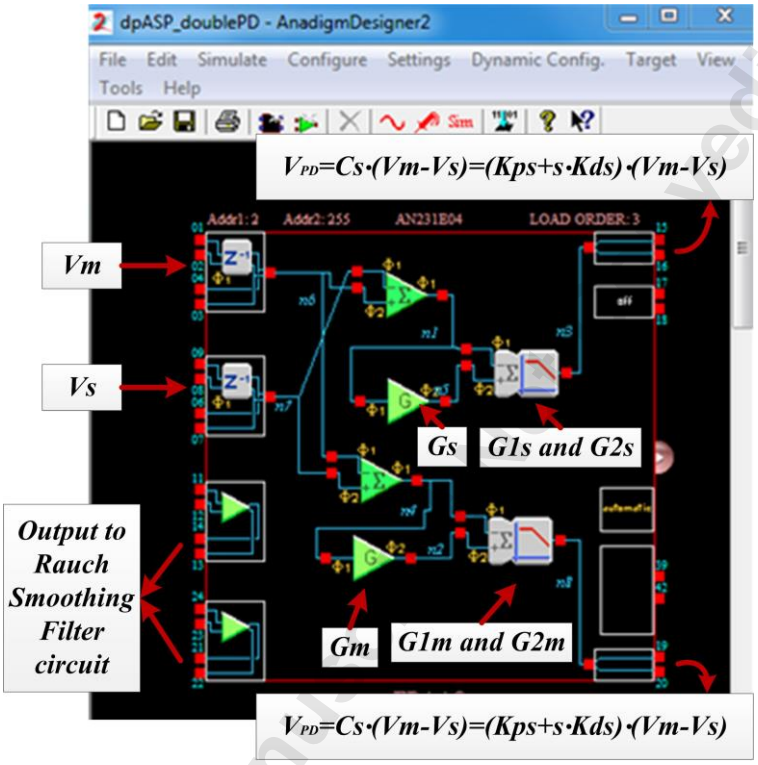

Fig. 6. Circuit realization of PD controllers C_m or C_s .

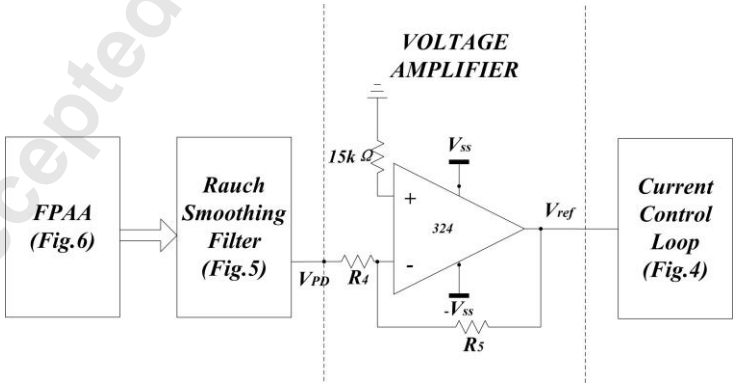

Fig. 7. Circuit diagram of analog position control.

Fig. 6 shows a circuit realization of analog PD controllers implemented using the AN231E04 FPAA device in the professional design software AnadigmDesigner 2.7.1. The master and slave robots positions V_m and V_s (i.e., the voltage readouts from the corresponding potentiometers) are inputs to Fig. 6. Each control circuit is composed of these Configurable Analog Modules (CAM) as shown in Fig. 8.

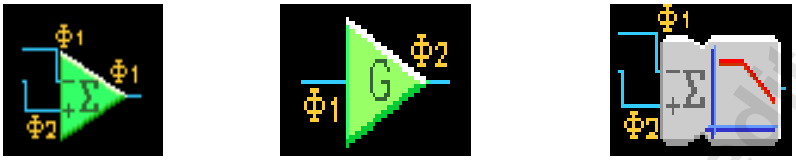

(a) SumDiff CAM (b) GainHalf CAM (c) SumFilt CAM

Fig. 8. Three Configurable Analog Modules (CAM) used for each control circuit.

The master and slave robots positions and (i.e., the voltage readouts from the corresponding potentiometers) are inputs to Fig. 6 (and Fig. 7). For the master robot, in the SumDiff CAM, V_s is added to $-V_m$ (the gains of the inputs in theSumDiff CAM can be chosen differently if position scaling between the master and slave robots is desired). Then, $V_s - V_m$ is input to the GainHalf CAM, which generates a phase-delayed half-cycle gain *Gm* to implement the differentiator required as part of the PD control. The proportional control is tuned by changing the gains *G1m* and *G2m* in the SumFilt CAM. A similar procedure happens on the slave side. Overall, the PD control gains for the master and the slave will be

$$\begin{aligned} K_{pm} &= G_{1m} - G_m \cdot G_{2m}\ , K_{dm} = \left(G_m \cdot G_{2m}\right)/F_c\ , \\ K_{ps} &= G_{1s} - G_s \cdot G_{2s}\ , K_{ds} = \left(G_s \cdot G_{2s}\right)/F_c\ , \end{aligned} \tag{27}$$

respectively, where K_{pm}, K_{ps} are the proportional gains, and K_{dm}, K_{ds} are the differential gains. Here, G_m, G_s are the gains of the GainHalf CAM for the master robot controller and the slave robot controller, respectively, G_{1m} and G_{2m} the input gains in the SumFilt CAM in the master side, while G_{1s} and G_{2s} are

the corresponding constants in the slave side, and F_c is the clock frequency.

Then, as shown in Fig. 7, the output voltages go through Rauch (also known as multiple feedback) differential filters [20] to smooth the control signals, which later need to be amplified to meet our task requirements. The reason to use another amplifier is that, the maximum output of the FPAA chip is 0.3 volt, while we need 1 to 10 volts for normal human operation, so we need extra amplifier. The voltage amplifier part has been marked on Fig.5, next to the Rauch Smoothing Filter. In Fig. 7, V_{PD} represents the voltage output from the FPAA-based PD controller after being filtered. Overall, assuming a unity gain for the Rauch Smoothing Filter block, the master and slave controllers' transfer functions incorporating the FPAA-based PD Controllers of Fig. 6 and the Voltage Amplifier blocks of Fig. 7 will be

$$\begin{aligned} C_m &= \frac{R_5}{R_4}\left(K_{pm} + s \cdot K_{dm}\right) = K_{m\_CT} + s \cdot B_{m\_CT}\,, \\ C_s &= \frac{R_5}{R_4}\left(K_{ps} + s \cdot K_{ds}\right) = K_{s\_CT} + s \cdot B_{s\_CT} \end{aligned} \tag{28}$$

4.2: Stability range of hybrid bilateral controller

A series of experiment were conducted to find the maximum stable control gains under different sampling times. The damping *b* of the robots can be found through grey-box system identification [10], which yields $b_m = b_s = 0.0018$. The sampling time for the digital controller is changed between 1*ms* and 1*s*.

When $T = 0.001s$, $b_m = b_s = 0.0018$, $B_{m\_DT} = B_{s\_DT} = 0$, the equation (26) became

$$0.0009 + B_{CT} > \frac{K_{DT}}{2} \times 0.001 \tag{29}$$

which is the relationship between B_{CT} and K_{DT}.

Journal of Dynamic Systems, Measurement and Control. Received September 25, 2015;
Accepted manuscript posted May 29, 2018. doi:10.1115/1.4040440

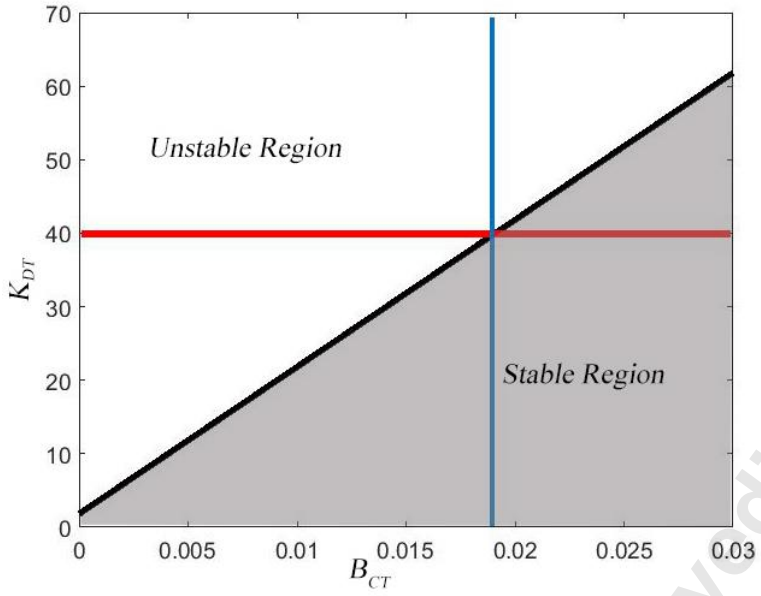

Fig. 9 The relationship between B_{CT} and K_{DT} based on the theoretical absolute stability

When we chose proportional gain $K_{m\_CT} = K_{s\_CT} = 10$, which helps to meet the high-gain condition of our two-teleoperation task case, according to Fig. 6, Fig. 7 and gain equation (27) [20], $B_{CT} < 0.03$ is acceptable, thus we chose $B_{m\_CT} = B_{s\_CT} = 0.025$.

In the experiments, the master robot is manipulated by a human operator while the slave robot is in free motion. If the master's and/or the slave's positions become unbounded or indefinitely oscillating, the teleoperation system is judged to be unstable. Conversely, if the robots' positions remain bounded, the teleoperation system is judged to be stable. At each tested sampling period, the unstable experiment with the minimum digital proportional control gain ($K_{m\_DT} = K_{s\_DT}$) is marked by a square in Fig. 10. Also, at each tested sampling period, the stable experiment with the maximum digital control gain is marked by a star in Fig. 10. The theoretical stability borderline (26) is also shown by a solid line in Fig. 10. As expected, the experimentally-obtained squares and stars lie close to the theoretically-derived stability boundary. In the above tests, the digital controllers had no damping ($B_{m\_DT} = B_{s\_DT} = 0$).

Journal of Dynamic Systems, Measurement and Control. Received September 25, 2015;
Accepted manuscript posted May 29, 2018. doi:10.1115/1.4040440

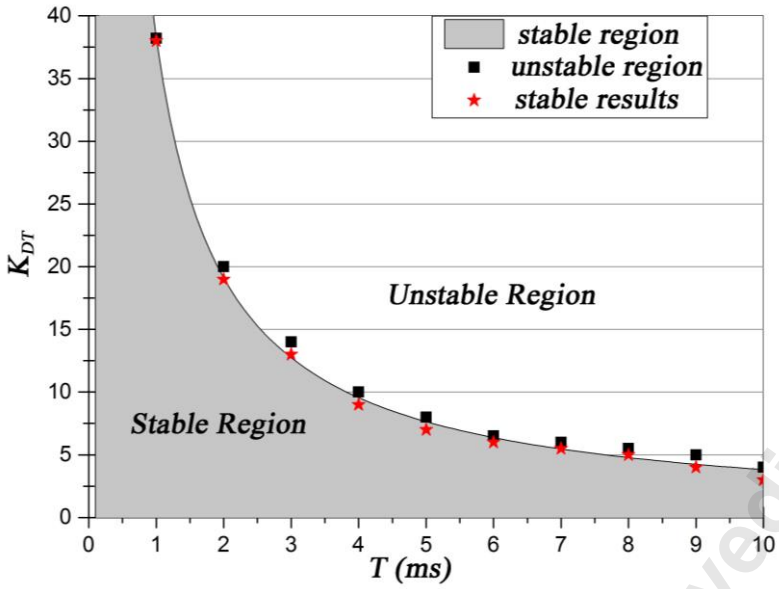

Fig. 10. The theoretical absolute stability region in K_{DT}-T plane versus experimental data points obtained from tests on the hybrid controlled teleoperator.

4.3 Case study I: Teleoperated switch flipping

4.3.1: Experiment design

In order to demonstrate the superior performance of the proposed hybrid controller compared to the case of pure digital control or pure analog control, a switch flipping task is considered. Consider a teleoperated switch-flipping task, where the user needs to flip the switch in Fig. 11 from position 1 to position 2 but not to position 3. In order to achieve this aim in the teleoperation mode, the master/slave position tracking error, which is influenced by the teleoperation controller performance, should be no more than the distance between positions 2 and 3 of the switch. Evidently, successful user task performance requires high teleoperation system transparency.

The purpose of this case is to study if narrowing the effect of sampling on controller can enhance the teleoperated task performance and if our proposed method has the best task performance under the same conditions. Firstly, we apply the same input force on the master side to eliminate the effect from

human operator, and to do a fair comparison of system performance between different controllers, in this way, we can study the effect of sampling in teleoperation task without human-made influence. Secondly, as can be seen from equation (18), the complete formula should include the input force from human operator, thus on this case and case in section 4.3, we both invited human operator to accomplish teleoperated task.

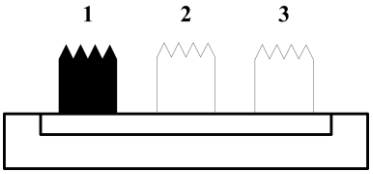

Fig. 11. A three-way switch.

In the following, the hybrid controller is evaluated in terms of system performance and human task performance. The system performance is measured in terms of the master-slave position tracking error, which as described above is key to successful performance of the switch-flipping task. The human task performance is measured by human factors experiments in which the success rate of human subjects in performing the switch-flipping task is measured.

To evaluate the system performances under various controllers, there is a need to eliminate the influence of the human operator for a fair comparison. The arrangement in Fig. 12 is used to replace the human operator, where a weight *m* is connected to the handle of the master robot through a pulley and rope mechanism. Evidently, the "operator" force applied on the master robot is always the same across different experiments. In this way, it is possible to do a fair comparison of system performance between different controllers.

Journal of Dynamic Systems, Measurement and Control. Received September 25, 2015;
Accepted manuscript posted May 29, 2018. doi:10.1115/1.4040440

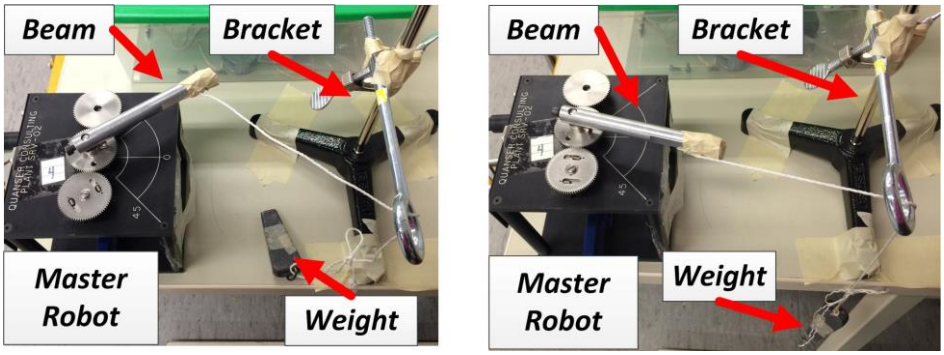

Fig. 12. Achieving repeatable inputs applied to the master robot.

4.3.2: Results

Fig. 13 shows the master-slave position tracking errors of three systems – analog controlled, digital controlled, and hybrid controlled – with their maximum admissible (i.e., stability-preserving) control gains when the slave robot hits a stiff wall. It can be seen that for the same input force applied on the master robot, the position tracking errors between the master robot and the slave robot are 0.05, 0.09 and 0.21 under hybrid, pure analog, and pure digital control, respectively. Comparing the first and the third numbers, it is seen that partially relieving the teleoperation system from the sampling-imposed limitations in terms of the control gain upper bound (by including an analog controller) has a significant effect on the system performance. Comparing the first and the second numbers, we see that the constraints imposed by op-amp saturation in the case of pure analog control limit the tracking performance that is achievable as compared to the case of hybrid control. Next, we will investigate if better system performance also translates into higher task performance success rates.

Journal of Dynamic Systems, Measurement and Control. Received September 25, 2015;
Accepted manuscript posted May 29, 2018. doi:10.1115/1.4040440

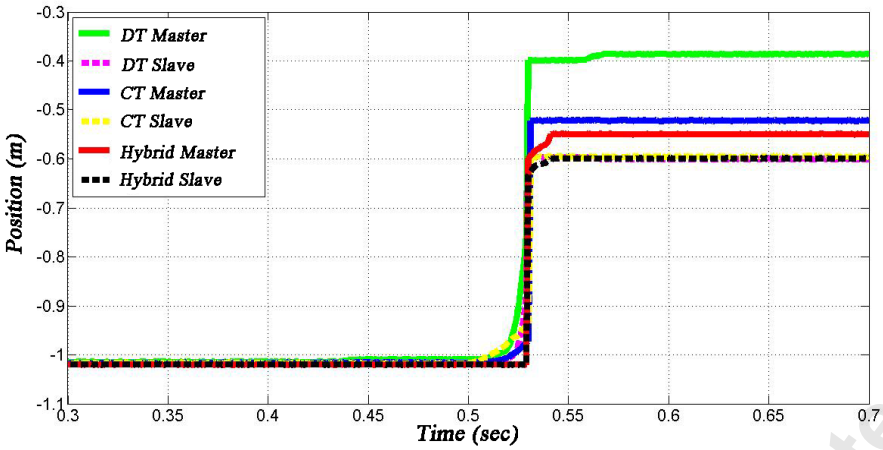

Fig. 13. Position tracking profiles achieved with various controllers when the slave has hit a rigid wall.

Five human operators (two females and three males) were asked to flip the switch shown in Fig. 11. They had modest prior knowledge about the teleoperated three-way switch task. The human operators could only manipulate the master robot and the slave robot was the one to interact with the switch. The operator's primary goal was defined as flipping the switch in Fig. 11 from position 1 to position 2 but not to position 3 by applying appropriate forces on the master side. The operators were told that they had 3 seconds to finish the task, which was found to be enough time.

Each operator performed five sets of trials with a short break (5-10 seconds) between each two trials. In each trial, one of three different conditions (1. hybrid control in which the digital control had a 1ms sampling period, 2. analog control, 3. digital control with a 1ms sampling period) was presented to an operator for doing the switch-flipping task. Therefore, each user performed a total of 15 trials. The trials were presented in a randomized order to each operator. Before the experiments, each operator was given two to three practice trials until he or she felt comfortable with the operation of the master-slave system and understood the switch-flipping task.

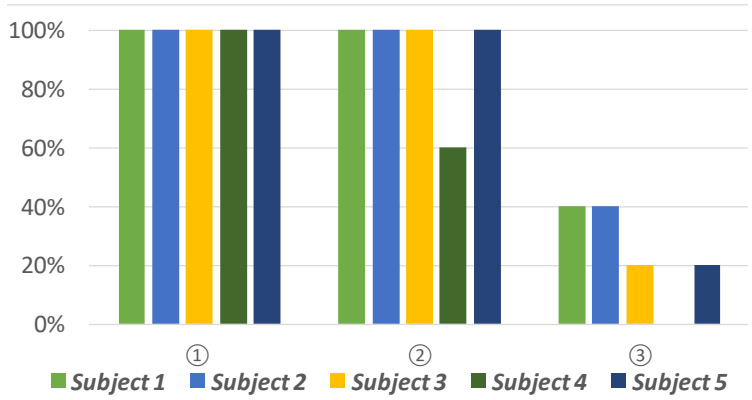

Fig. 14. Success rates of tasks under different control conditions.

4.3.3: Discussion

The final results, averaged over the 15 trials for each subject, are presented graphically in Fig.14. The human participants could successfully flip the switch from state 1 to state 2 in

(1) 100% of times when using the hybrid analog/digital controlled teleoperation system ①.

(2) 60-100% of times when using the pure analog controlled teleoperation system ②.

(3) 0-40% of times when using the digital controlled teleoperation system with a sampling period of 1ms ③.

Therefore, with a hybrid-controlled teleoperation system, the operators had the least problem with performing the task. With a pure analog controlled teleoperation system, the task success rates go down due to an inability to have high control gains (due to analog circuit saturation) that are required for small position tracking errors. This problem is exacerbated when using a pure digital controller.

To ensure that the averages of success rates reported above can be relied upon, tests of statistical significance (right-tailed t-test) were performed. Overall, ①>②>③ can be concluded where ">" signifies higher success rates. This is because of the corresponding p-values, which are 0.0445 between ① and ②,

0.000015 between ① and ③, are all less than 0.05, confirming the existence of significant differences between the corresponding pairs. This means that the task success rate is much higher in hybrid-controlled teleoperation than in pure analog and digital controlled teleoperation.

4.2: Case Study II: Object Stiffness Discrimination

4.4.1: Experiment design

In order to compare the system's impedance reflection performance between the various controllers for the bilateral teleoperation system, experiments were conducted in which the task is for the operator to discriminate between two objects of different stiffness (harder and softer) through telerobotic palpation. This has applications in many domains such as tissue palpation for localizing cancerous tissue. For the human operator to perform the tasks successfully in the teleoperation mode, it is important to ensure that the impedance perceived by the human operator highly resembles the palpated object's stiffness. Thus, if one or both of the objects have a high stiffness, the teleoperation system needs to reflect to the human operator a high impedance, which again requires high control gains in the robots.

Note that while the slave robot's controller gain needed to be high in Case Study I for ensuring small position tracking error and thus successful task performance, it is the master robot's controller gain that needs to be high in Case Study II for stiff impedance reflection and thus successful task performance. Nonetheless, since the master and robots are similar in our experimental setup, we use the same control gain for both the master and the slave.

Five subjects (three males and two females) participated in our experiments. The subjects had average exposure to haptic teleoperation. The subjects' primary goal was defined as distinguishing objects in terms of their relative stiffness without visual and audio feedback. After an object was probed using the teleoperation system by a human participant, it was replaced with a different or the same object. After

probing the second sample again through the teleoperation system, the participant had to declare if the first object was harder, softer, or the same as the second object.

The master-slave setup used in this experiment is shown in Fig. 15. The hard object is a block of wood, and the other object is a block of compressed packaging foam. Both objects have high stiffnesses with a small difference between the two (the wood is closer to $Z_e \to \infty$). Thus, it is important for the teleoperation system to truthfully reflect high impedances to the human operator who is probing an unknown object through the teleoperation system. In each trial, one out of the three different controllers (1. hybrid analog/digital controller, 2. pure analog controller, 3. pure digital controller) and two objects (the hard and soft objects in different orders or the same object twice) were presented to the operator. Whenever a digital controller was used, a 1 ms sampling period was utilized. Each participant performed a total of 27 trials with a short break between them. The trials were presented in a randomized order to each operator. Before the experiments, each operator was given two to three practice trials until he or she felt comfortable with the operation of the master-slave system and understood the task. The operators were told that they had 30 seconds to finish the task, which was found to be enough time.

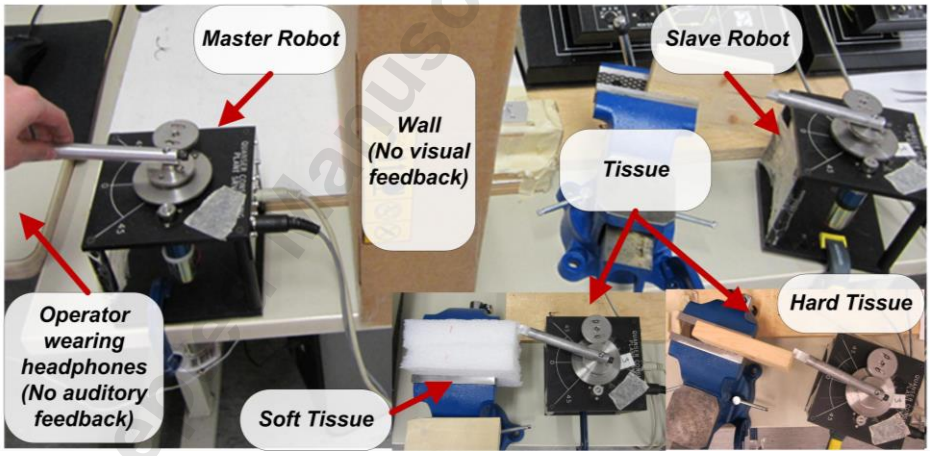

Fig. 15. Master-slave setup for performing telemanipulated object stiffness discrimination task.

4.4.2: Results

The final results, averaged over the 27 trials for each subject, are presented graphically in Fig. 16.

Journal of Dynamic Systems, Measurement and Control. Received September 25, 2015;
Accepted manuscript posted May 29, 2018. doi:10.1115/1.4040440

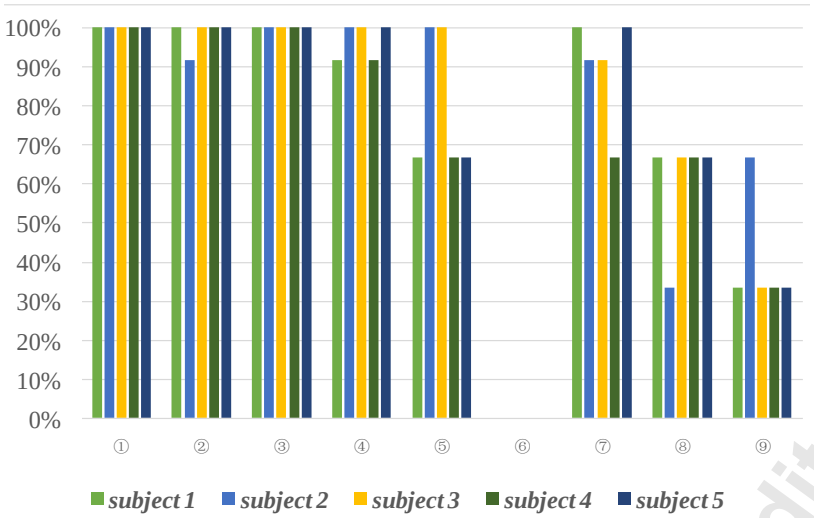

Fig. 16. Success rates of the task under different control conditions.

The cases ①, ④ and ⑦ correspond to hybrid analog/digital controlled teleoperation. The cases ②, ⑤ and ⑧ correspond to the teleoperation system with a pure analog controller. The cases ③, ⑥ and ⑨ correspond to teleoperation system with a pure digital controller. In cases ① to ③, the softer object was presented twice to the operator. In cases ④ to ⑥, the harder object was presented twice to the operator. In cases ⑦ to ⑨, two objects with different stiffnesses were presented to the operator in a random order.

As it can be seen, the success rate in hybrid method-controlled teleoperation system is the highest. According to the feedback from operators, they could always feel the stiffest reflected impedance with the hybrid controller than with the other two controllers. Under digital control, the harder object feels like the softer one due to significantly lower control gains as required for stability, thus explaining for zero success rates in cases ⑥.

In order to analyze the statistical significance of the results shown in Fig. 16, right-tailed t-test between different pairs of controllers is used for further investigation. The p-value for the t-test between ① and ② and between ① and ③ are higher than the selected threshold value of statistical significance (0.05). This implies that there exists no statistical difference among the three different controllers when probing the softer object twice – all controllers manage to give sufficient feeling to the subjects to perform

the task with high success rates. The p-value of ④ versus ⑤ and ④ versus ⑥ are 0.00375 and 0.00000059, respectively, indicating the statistical significance of higher success rates for hybrid controller compared to the pure analog or digital controller when probing the harder object twice. The other two right-tailed t-tests between ⑦ and ⑧ ($p = 0.0164$), and between ⑦ and ⑨ ($p = 0.0231$) also confirm the existence of significant differences between the corresponding pairs, indicating the better performance of hybrid analog/digital controller in distinguishing different stiffnesses. Overall, the task success rate is much higher in hybrid analog/digital based teleoperation than in pure analog or digital controlled teleoperation even for a small sampling period (1 ms) when dealing with stiff objects.

4.4.3: Discussion

It can be observed from the results that, all three different controllers can accomplish the probing task with the softer object; however, large errors can be introduced when dealing with the harder object if the proposed hybrid analog/digital controller is not used. The worst performance happens when using the pure digital control. The hybrid analog/digital controlled bilateral teleoperation system proves to be much better in transmitting task-related information (transmitted impedance) than the pure analog or digital controlled teleoperation system.

We need to notice, as the man-made force has been considered in our tasks, the control transparency can be better explored if the manipulators are more familiar and proficient with our task.

5: Conclusion

In this article, the performance of a hybrid analog/digital controlled bilateral teleoperation system was contrasted to that of a digital controlled and an analog controlled teleoperation system in theory and experiments. The work showed that the combination of analog and digital controllers can outperform the

traditional controllers in terms of system stability, system performance, and task success rates by enlarging the control gain range of the system. It also affords higher flexibility in terms of tuning the control gains by providing two channels for doing that.

One possible extension of the current study includes applying the hybrid controller to achieve highly transparent and stable teleoperation in haptic applications involving both force and position control, which can program complex algorithm while keeping the analog advantage.

FPAA can realize the dynamic parameter changes during the experiment and show more flexibility of the controller in bilateral teleoperation system, which can be a second extension of our work.

6: Acknowledgments

This research was supported by the Natural Sciences and Engineering Research Council (NSERC) of Canada under Grant RGPIN372042 and Grant RGPIN03907, by the Canada Foundation for Innovation (CFI) under Grant LOF28291, by the Innovative Research Groups of the National Natural Science Foundation of China under Grant 51521003, by Self-Planned Task of State Key Laboratory of Robotics and System (HIT) under Grant SKLR201403bB, by the China Scholarship Council (CSC) under Grant [2013]06120200, by Jiangsu Postdoctoral Science Foundation under Grant 1601080C, by Jiangsu University Natural Science Foundation under Grant 17KJB310015, by Talented Scientific Research Foundation of Xuzhou Medical University under Grant D2015001 and D2017020. All of these funds involving human subjects' experiments.

7: References

[1] Toiserkan, K.G., 2014, "A unified haptic framework for rendering stiff and dynamic virtual environments," PhD thesis, McGill University.

[2] Imaidaa, T., and Sendaa, K., 2015, "Performance improvement of the PD-based bilateral teleoperators with time delay by introducing relative D-control," Advanced Robotics, 29, (6), pp. 385-400.

[3] Rahimia, H.N., and Nazemizadehb, M., 2014, "Dynamic analysis and intelligent control techniques for flexible manipulators: a review," Advanced Robotics, 28, (2), pp. 63-76.

[4] Walters, M.L., Lohse, M., Hanheide, M., Wrede, B., Syrdal, D.S., Koay, K. L., Green, A., Huttenrauch, H., Dautenhahn, K., Sagerer, G., and Eklundh, K. S., 2011, "Evaluating the robot personality and verbal behavior of domestic robots using video-based studies," Advanced Robotics, 2011, 25, (18), pp. 2233-2254.

[5] Li, J. Q., Sang, H. Y., Han, Y. Y., Wang, C. G., and Gao, K. Z., 2018, "Efficient multi-objective optimization algorithm for hybrid flow shop scheduling problems with setup energy consumptions," Journal of Cleaner Production, 2018, (181), pp. 584-598.

[6] Duan, P. Y., Li, J. Q., Wang, Y., Sang, H. Y., Bao, X. J., 2018, "Solving chiller loading optimization problems using an improved teaching-learning-based optimization algorithm," Optimal Control Applications & Methods. 39, (1), pp. 65-77.

[7] Xu, W. Z., Yu, H., Lu, D. J., Liu, F., and Liu, Z. Y., 2018, "A Novel Data Reuse Method to Reduce Demand on Memory Bandwidth and Power Consumption for True Motion Estimation," IEEE Access, 6, pp. 10151-10159.

[8] Gillespie, B., and Cutkosky M., 1996, 'Stable user-specific rendering of the virtual wall'. Proceedings of the ASME Int. Mechanical Engineering Conf. and Exposition. Atlanta, GA, pp. 397–406.

[9] Leung, G., and Francis, B., 1992, "Bilateral control of teleoperators with time delay through a digital communication channel," Proc. of the Thirtieth Annual Allerton Conference on Communication, Control and Computing, pp. 692–701.

[10] Jazayeri, A., and Tavakoli, M., 2013, "Absolute stability analysis of sampled-data scaled bilateral teleoperation systems," Control Engineering Practice, 21, (8), pp. 1053-1064.

[11] Lee, D. J., and Spong, M. W., 2006, "Passive bilateral teleoperation with constant time delay," IEEE Trans. on Robotics, 22, (7), pp. 269-281.

[12] Secchi, C., Stramigioli, S., and Fantuzzi, C., 2007, "Control of Interactive Robotic Interfaces: A Port-Hamiltonian Approach (Springer Tracts in Advanced Robotics)," Springer-Verlag New York, Inc., Secaucus, NJ, USA.

[13] Berestesky, P., Chopra, N., and Spong, M., 2004, "Discrete time passivity in bilateral teleoperation over the Internet," Proc. of Int. Conf. on Robotics and Automation, New Orleans, LA, pp. 4557–4564.

[14] Aziminejad, A., Tavakoli, M., Patel, R.V., and Moallem, M., 2008, "Stability and performance in delayed bilateral teleoperation: Theory and Experiments," Control Engineering Practice, 11, (16), pp. 1329-1343.

[15] Nealen, A., Muller, M., Keiser, R., Boxerman, E., and Carlson, M., 2006, "Physically based deformable models in computer graphics," Computer Graphics Forum, 25, pp. 809-836.

[16] Courtecuisse, H., Jung, H., Allard, J., Duriez, C., Lee, D. Y., and Cotin, S., 2010, "GPU-based real-time soft tissue deformation with cutting and haptic feedback," Progress In Biophysics & Molecular Biology, 2010, 12, (103), pp. 159-168.

[17] Mafi, R., Sirouspour, S., Mahdavikhah, B., Elizeh, K., Kinsman, A., and Nicolici, N., 2010, "A parallel computing platform for real-time haptic interaction with deformable bodies," IEEE Transactions on Haptics, (3), pp. 211-223.

[18] Susa, I., and Takehana, Y., 2014, "Haptic Rendering based on Finite Element Simulation of Vibration," IEEE Haptics Symposium 2014, 2, pp. 23-26.

[19] Kawai, M., and Yoshikawa, T., 2004, "Haptic display with an interface device capable of continuous-time impedance display within a sampling period," IEEE/ASME Transactions on Mechatronics, 9, (1), pp. 58-64.

[20] AnadigmDesigner@2 User Manual, 2004, Anadigm Inc., Mesa, AZ.

[21] Malcher, A., and Falkowski, P., 2014, "Analog reconfigurable circuits," Int. Journal of Electronics and Telecommunications, 60, (1), pp. 15-26.

[22] Ogata, K., 1995, "Discrete-time control systems," Prentice Hall, 2nd edn.

[23] Jazayeri, A., and Tavakoli, M., 2010, "Stability analysis of sampled-data teleoperation systems," 49th IEEE Conference on Decision and Control (CDC), pp. 6.

[24] Jazayeri, A., and Tavakoli, M., 2011, "A passivity criterion for sampled data bilateral teleoperation systems," Proc. of IEEE World Haptics Conference, Istanbul, Turkey, pp. 487–492.

[25] Khalil, H., 2002, "Nonlinear Systems," Prentice Hall.

[26] Hitz, L., and Anderson, B. D. O., 1969, "Discrete positive-real functions and their application to system stability," Proc. of the Institution of Electrical and Engineers, 116, (1), pp. 153–155.

[27] Astrom, K. J., and Wittenmark, B., 1994, "Adaptive control," Addison-Wesley Longman Publishing Co., Inc., Boston, MA, USA, 2nd edn.

[28] Colgate., J., and Schenkel, G., 1997, "Passivity of a class of sampled-data systems: Application to haptic interfaces," Journal of Robotic Systems, 14, (1), pp. 37-47.

[29] Yang, T., Fu, Y. L., and Tavakoli, M., 2015, "Digital versus analog control of bilateral teleoperation system: a task performance comparison," Control Engineering Practice, 38, pp. 46-56.

Journal of Dynamic Systems, Measurement and Control. Received September 25, 2015;
Accepted manuscript posted May 29, 2018. doi:10.1115/1.4040440

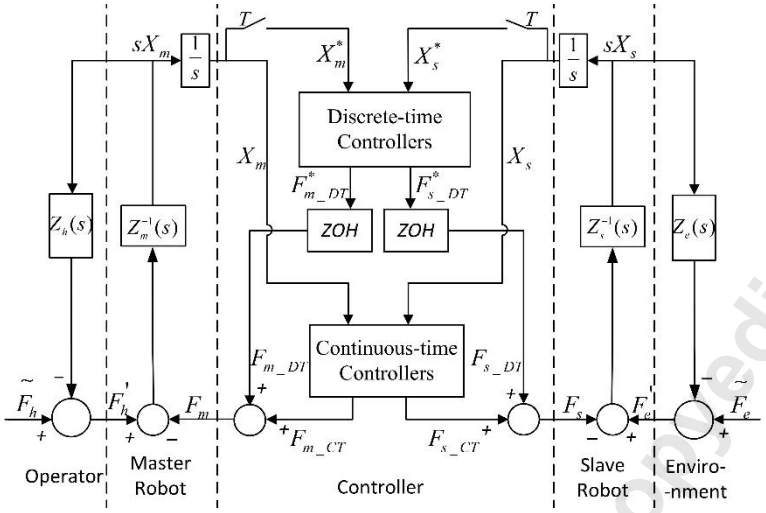

Fig. 1: A PEB bilateral teleoperation system with a hybrid continuous-time (analog) and discrete-time (digital) controller.

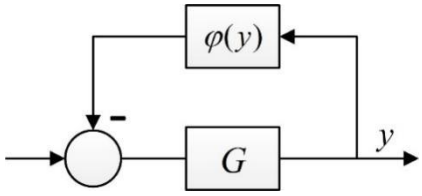

Fig. 2: A sampled-data feedback system with LTI system G in the forward path and nonlinearity $\varphi = \varphi(y)$ in the feedback path.

Journal of Dynamic Systems, Measurement and Control. Received September 25, 2015;
Accepted manuscript posted May 29, 2018. doi:10.1115/1.4040440

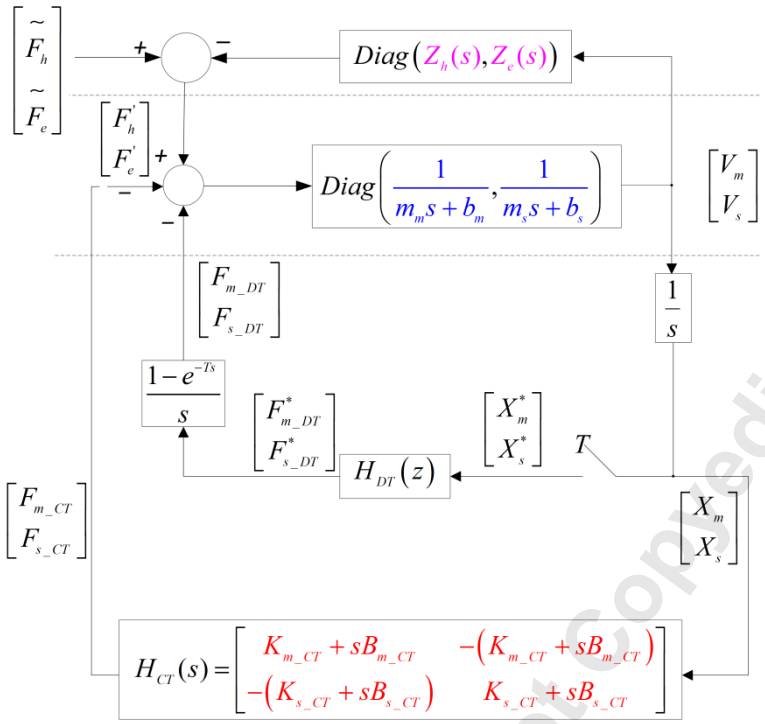

Fig. 3: Block diagram of the hybrid-control PEB bilateral teleoperation system.

Journal of Dynamic Systems, Measurement and Control. Received September 25, 2015;
Accepted manuscript posted May 29, 2018. doi:10.1115/1.4040440

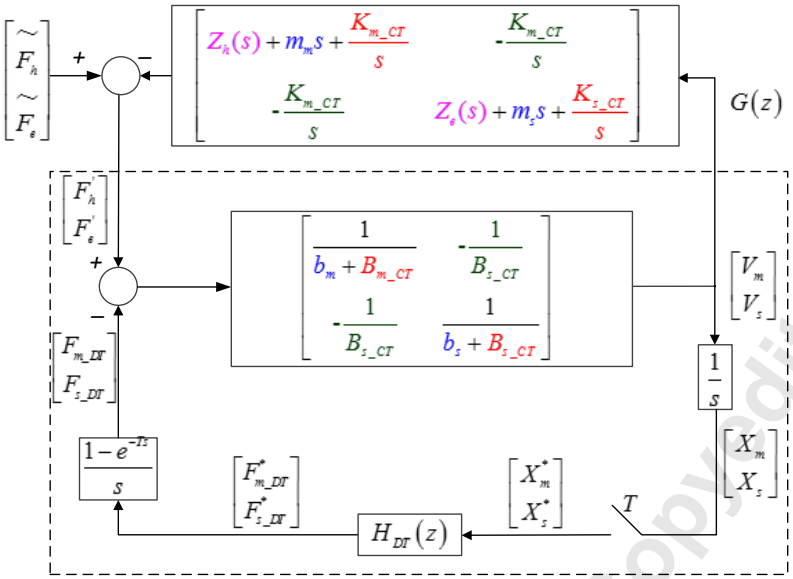

Fig. 4: Modified block diagram of Fig. 3.

Journal of Dynamic Systems, Measurement and Control. Received September 25, 2015;
Accepted manuscript posted May 29, 2018. doi:10.1115/1.4040440

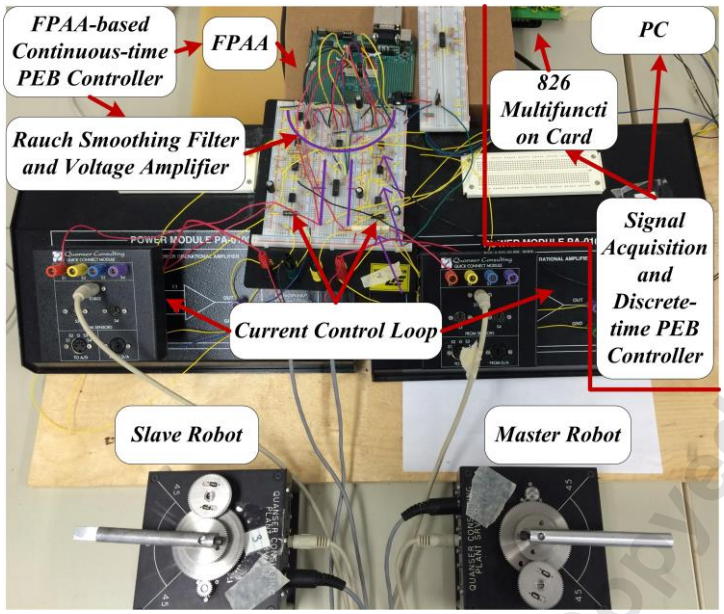

Fig. 5. The experimental bilateral teleoperation system.

Journal of Dynamic Systems, Measurement and Control. Received September 25, 2015;
Accepted manuscript posted May 29, 2018. doi:10.1115/1.4040440

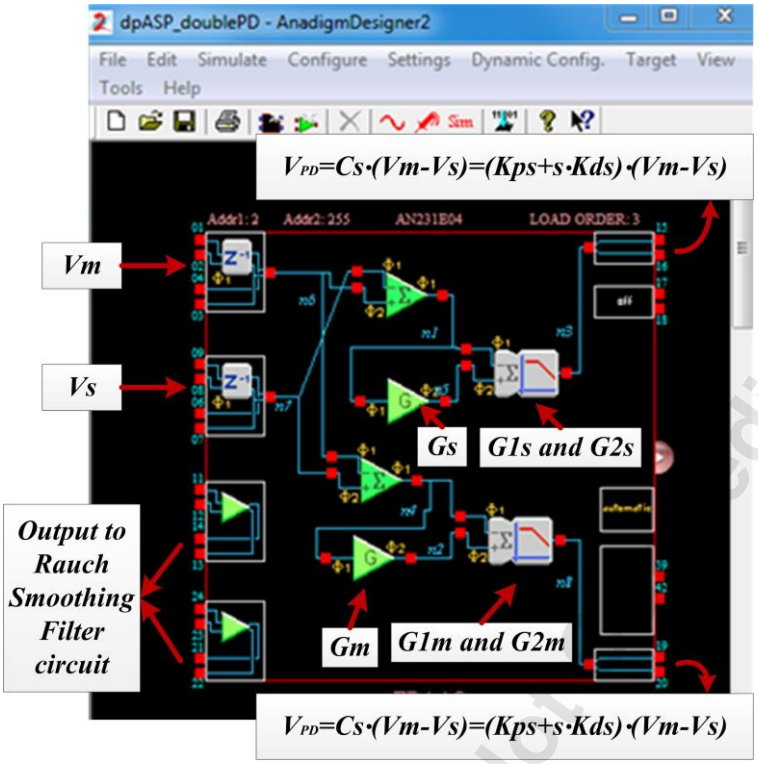

Fig. 6. Circuit realization of PD controllers C_m or C_s .

Journal of Dynamic Systems, Measurement and Control. Received September 25, 2015;
Accepted manuscript posted May 29, 2018. doi:10.1115/1.4040440

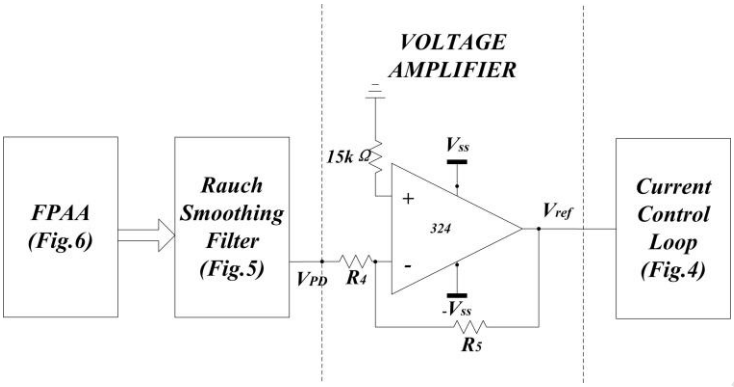

Fig. 7. Circuit diagram of analog position control.

Journal of Dynamic Systems, Measurement and Control. Received September 25, 2015;
Accepted manuscript posted May 29, 2018. doi:10.1115/1.4040440

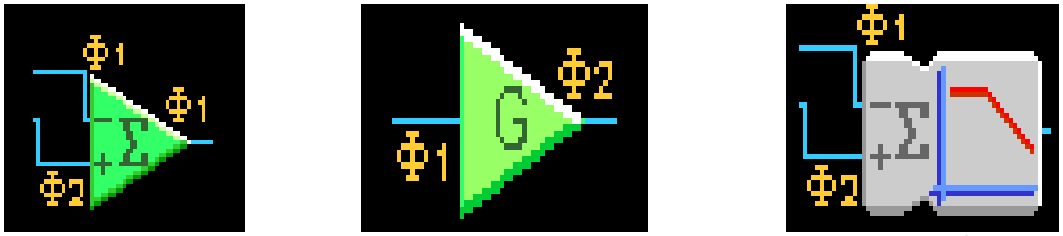

(a) SumDiff CAM (b) GainHalf CAM (c) SumFilt CAM

Fig. 8. Three Configurable Analog Modules (CAM) used for each control circuit.

Journal of Dynamic Systems, Measurement and Control. Received September 25, 2015;
Accepted manuscript posted May 29, 2018. doi:10.1115/1.4040440

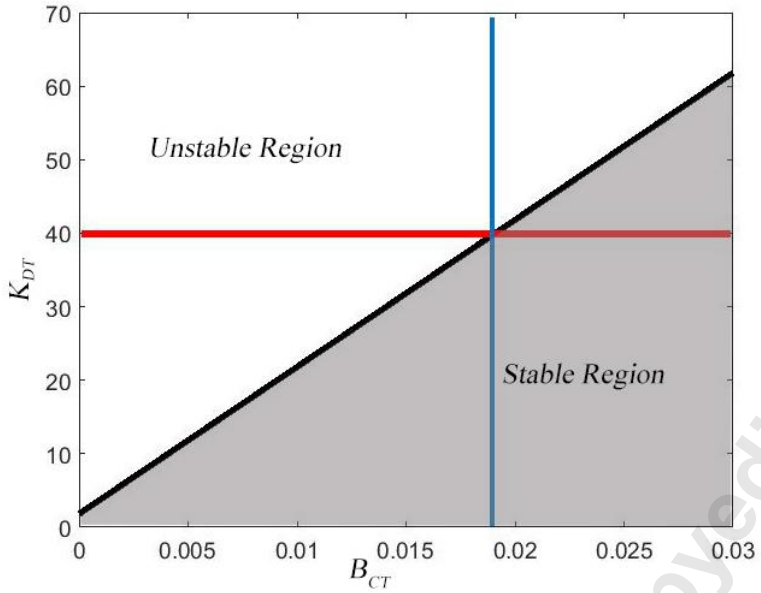

Fig. 9 The relationship between B_{CT} and K_{DT} based on the theoretical absolute stability

Journal of Dynamic Systems, Measurement and Control. Received September 25, 2015;
Accepted manuscript posted May 29, 2018. doi:10.1115/1.4040440

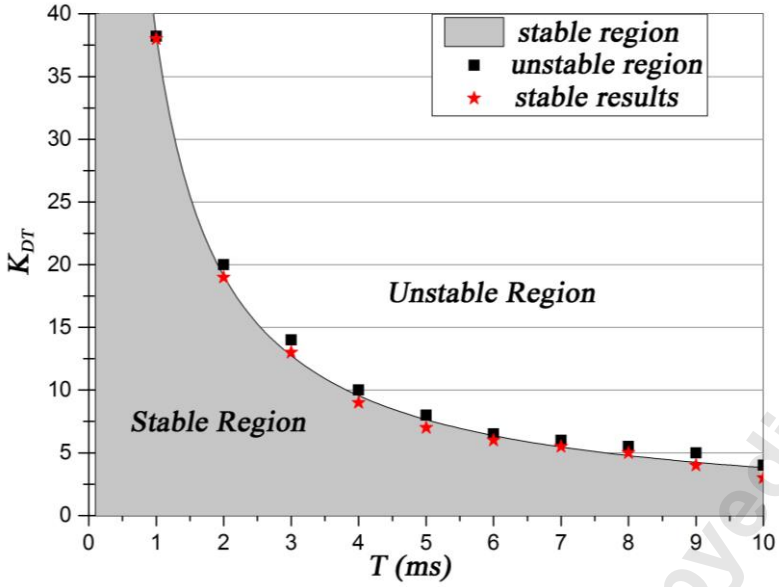

Fig. 10. The theoretical absolute stability region in K_{DT}-T plane versus experimental data points obtained from tests on the hybrid controlled teleoperator.

Journal of Dynamic Systems, Measurement and Control. Received September 25, 2015;
Accepted manuscript posted May 29, 2018. doi:10.1115/1.4040440

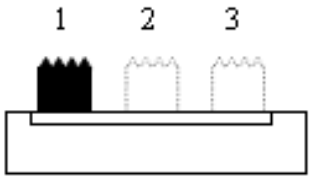

Fig. 11. A three-way switch.

Journal of Dynamic Systems, Measurement and Control. Received September 25, 2015;
Accepted manuscript posted May 29, 2018. doi:10.1115/1.4040440

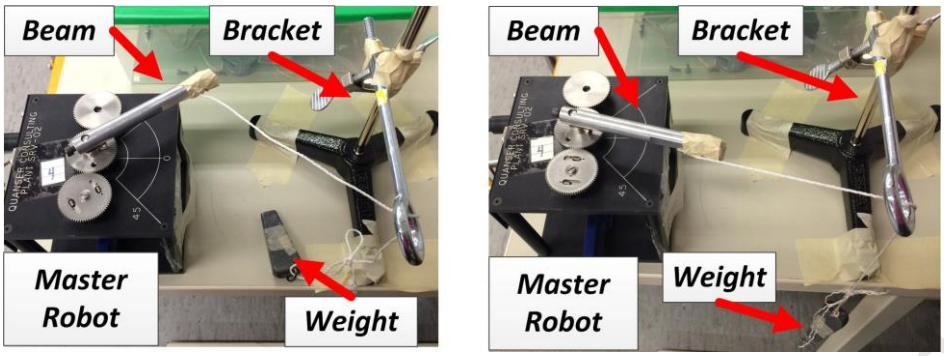

Fig. 12. Achieving repeatable inputs applied to the master robot.

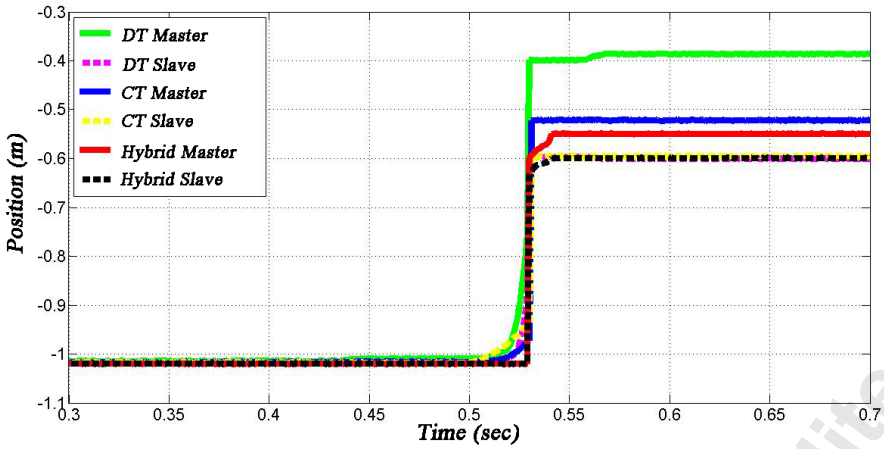

Fig. 13. Position tracking profiles achieved with various controllers when the slave has hit a rigid wall.

Journal of Dynamic Systems, Measurement and Control. Received September 25, 2015;
Accepted manuscript posted May 29, 2018. doi:10.1115/1.4040440

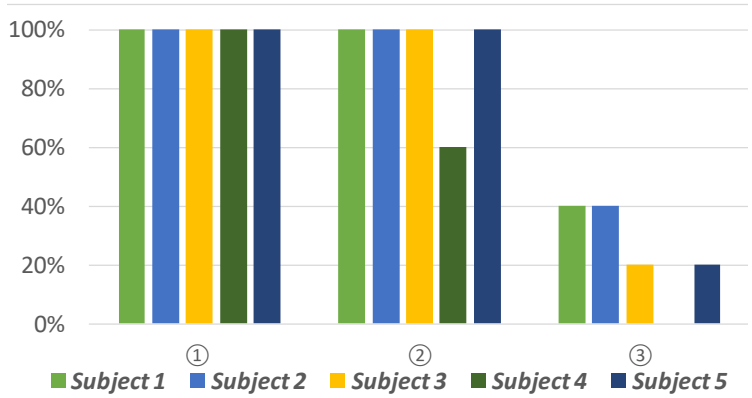

Fig. 14. Success rates of tasks under different control conditions.

Journal of Dynamic Systems, Measurement and Control. Received September 25, 2015;
Accepted manuscript posted May 29, 2018. doi:10.1115/1.4040440

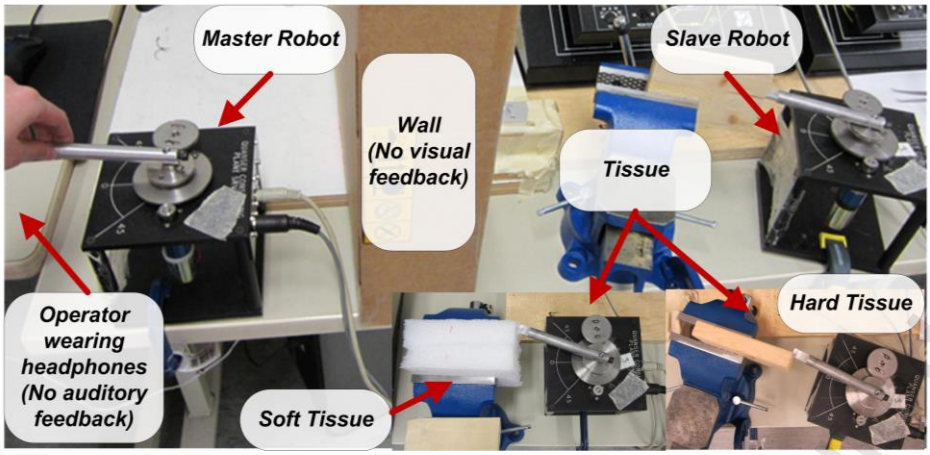

Fig. 15. Master-slave setup for performing telemanipulated object stiffness discrimination task.

Journal of Dynamic Systems, Measurement and Control. Received September 25, 2015;
Accepted manuscript posted May 29, 2018. doi:10.1115/1.4040440

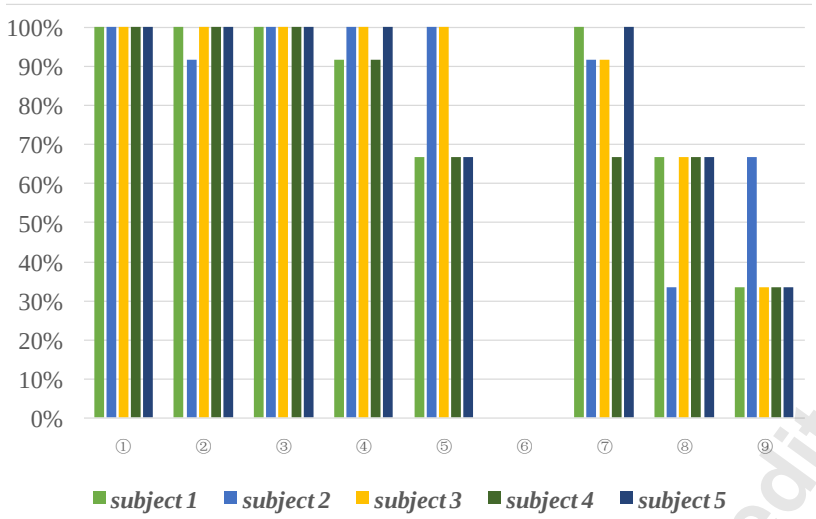

Fig. 16. Success rates of the task under different control conditions.